Photonic Circuits for Generating Modal, Spectral, and Polarization Entanglement
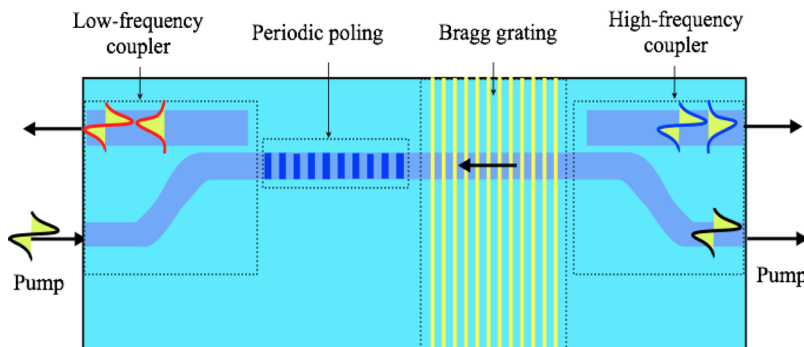
Mohammed F. Saleh,
Giovanni Di Giuseppe,
Bahaa E. A. Saleh, Life Fellow, IEEE
Malvin Carl Teich, Life Fellow, IEEE

Photonic Circuits for Generating Modal, Spectral, and Polarization Entanglement

Mohammed F. Saleh,[1] **Giovanni Di Giuseppe,**[2,3]
Bahaa E. A. Saleh,[1,2] *Life Fellow, IEEE*, **and**
Malvin Carl Teich,[1,4,5] *Life Fellow, IEEE*

[1]Quantum Photonics Laboratory, Department of Electrical and Computer Engineering,
Boston University, Boston, MA 02215 USA
[2]Quantum Photonics Laboratory, College of Optics and Photonics (CREOL),
University of Central Florida, Orlando, FL 32816 USA
[3]School of Science and Technology, Physics Division, University of Camerino, 62032 Camerino (MC), Italy
[4]Department of Physics, Boston University, Boston, MA 02215 USA
[5]Department of Electrical Engineering, Columbia University, New York, NY 10027 USA

Abstract: We consider the design of photonic circuits that make use of Ti:LiNbO$_3$ diffused channel waveguides to generate photons with various combinations of modal, spectral, and polarization entanglement. Down-converted photon pairs are generated via spontaneous parametric down-conversion (SPDC) in a two-mode waveguide (TMW). We study a class of photonic circuits comprising: 1) a nonlinear periodically poled TMW structure; 2) a set of single-mode waveguide (SMW)- and TMW-based couplers arranged in such a way that they suitably separate the three photons comprising the SPDC process; and, for some applications, 3) a holographic Bragg grating that acts as a dichroic reflector. The first circuit produces two frequency-degenerate down-converted photons, each with even spatial parity, in two separate SMWs. Changing the parameters of the elements allows this same circuit to produce two nondegenerate down-converted photons that are entangled in frequency or simultaneously entangled in frequency and polarization. The second photonic circuit is designed to produce modal entanglement by distinguishing the photons on the basis of their frequencies. A modified version of this circuit can be used to generate photons that are doubly entangled in mode number and polarization. The third photonic circuit is designed to manage dispersion by converting modal, spectral, and polarization entanglement into path entanglement.

Index Terms: Photonic circuits, integrated-optics devices, channel waveguides, waveguide couplers, parametric down-conversion, quantum optics, nonlinear optics, entangled photons, dispersion management.

1. Introduction

Entanglement in a pair of photons can be manifested in degrees of freedom that are discrete, such as polarization [1], or in degrees of freedom that are continuous, such as spectral or spatial [2]–[5]. However, a continuous degree of freedom may be binarized by selection of a pair of values, as in path entanglement [6], [7], or, as in orbital-angular-momentum entanglement [8], by expansion in some basis while retaining only two basis functions [9]. Alternatively, in place of truncation, the space of

continuous functions of position may be mapped onto a binary set of even and odd functions, as in spatial-parity entanglement [10]–[12]. We recently investigated the possibility of using spontaneous parametric down-conversion (SPDC) in two-mode planar and circular waveguides to generate guided-wave photon pairs entangled in mode number [13]. If the photons are confined in this manner, the spatial variables are naturally binarized and can be used to represent a modal qubit [14].

In this paper, we consider the design of photonic circuits, based on Ti:LiNbO$_3$ diffused channel waveguides, that generate photon pairs endowed with various combinations of modal, spectral, and polarization entanglement. The on-chip generation of such photon pairs can serve as a basic resource for one-way quantum computation [15], as well as for linear optical quantum computing [16]. Down-converted photon pairs are generated via SPDC in a two-mode waveguide (TMW) using a CW pump source. The waveguide configuration confines the photons to a single direction of propagation. Any of the available degrees of freedom—mode number, frequency, or polarization— can be used to distinguish the down-converted photons, while the others can serve as carriers of entanglement. We study a class of photonic circuits that comprises: 1) a nonlinear periodically poled TMW structure; 2) a set of single-mode waveguide (SMW)- and TMW-based couplers arranged in such a way that they suitably separate the three photons comprising the SPDC process; and, for certain applications, 3) a holographic Bragg grating.

A good deal of effort has been devoted to examining the properties of single-mode silica-on-silicon waveguide quantum circuits [17], [18], with an eye toward applications in quantum-information processing [19]–[24]. For these materials, the photon-generation process necessarily lies off-chip, however. Single- and multi-mode potassium titanyl phosphate (KTiOPO$_4$, KTP) waveguide structures have also been extensively studied for producing pulsed SPDC [25]–[29], but it appears that only the generation process has been incorporated on-chip. Earlier, periodically poled lithium niobate (PPLN) waveguide structures were suggested for producing SPDC [30], and the conditions required to generate counterpropagating entangled photons from an unguided pump field were established [31]. Furthermore, the generation of non-collinear and non-degenerate polarization-entangled photons via concurrent Type-I parametric down-conversion was demonstrated in a PPLN crystal [32].

The use of lithium niobate photonic circuits has a number of merits: 1) The properties of the material are well-understood since it has low loss and has long been the basis of integrated-optics technology [33], [34, ch. 8]; and 2) the material can easily be periodically poled [35], [36] for the purpose of phase matching parametric interactions. In addition, as we show in this paper, 3) circuit elements such as mode-separation components can readily be designed for TMWs; and 4) the generation, separation, and processing of entangled photons can all be accommodated on a single chip. Moreover, consistency between simulation and experimental measurement has been demonstrated in a whole host of configurations [37]–[41]. To enhance tolerance to fabrication errors, photonic circuits can be equipped with electrooptic adjustments. For example, an electrooptically switched coupler with stepped phase-mismatch reversal serves to maximize coupling between fabricated waveguides [42], [43].

The paper is organized as follows. In Section 2, the theory of modal entanglement in TMWs is reviewed. Section 3 is dedicated to examining the operation of a photonic circuit that produces a pair of frequency-degenerate photons at its output. As explained in Section 4, changing the parameters of the elements comprising the circuit considered in Section 3 allows it to produce nondegenerate down-converted photons that are entangled in frequency or simultaneously entangled in frequency and polarization. The second photonic circuit, which is examined in Section 5, distinguishes the photons on the basis of their frequencies and provides means for generating modal entanglement and, with some modifications, modal and polarization double entanglement. The third photonic circuit, which is considered in Section 6, is designed to manage the deleterious effects of dispersion. The conclusion is provided in Section 7.

2. Generating Modal Entanglement in TMWs

The theory underpinning the generation of modal entanglement in waveguides was recently described [13]. Entanglement arises from the multiple possibilities for satisfying energy and

momentum conservation, as required by the parametric interaction process. In this section, we proceed to apply the theory provided in [13] to diffused channel Ti:LiNbO$_3$ waveguides.

Consider a SPDC process in a periodically poled TMW structure, in which a CW pump wave p propagating in the y-direction is down-converted into a signal wave s and an idler wave i [34, ch. 21]. The fundamental mode of this TMW ($m_q = 0$) is even while the next-higher mode ($m_q = 1$) is odd, where $q = p, s, i$. We seek to generate an entangled state such that if the signal is in the even mode, then the idler must be in the odd mode, and *vice versa*.

The biphoton state is written as [13]

$$|\Psi\rangle \sim \int d\omega_s \big[\Phi_{0,1,\sigma_s,\sigma_i}(\omega_s)|\omega_s, 0, \sigma_s\rangle|\omega_i, 1, \sigma_i\rangle + \Phi_{1,0,\sigma_s,\sigma_i}(\omega_s)|\omega_s, 1, \sigma_s\rangle|\omega_i, 0, \sigma_i\rangle \big] \tag{1}$$

where the squared-magnitude of $\Phi_{m_s,m_i,\sigma_s,\sigma_i}$ represents the SPDC spectrum associated with the $(m_s, m_i, \sigma_s, \sigma_i)$ component. The signal and idler mode numbers are m_s and m_i, their polarization indexes are σ_s and σ_i, and their angular frequencies are ω_s and ω_i, respectively, with $\omega_i = \omega_p - \omega_s$. The angular frequency of the pump is denoted ω_p. For ease of display, the output spectra for the two possibilities represented by the quantities $|\Phi_{0,1,\sigma_s,\sigma_i}(\omega_s)|^2$ and $|\Phi_{1,0,\sigma_s,\sigma_i}(\omega_s)|^2$ are normalized to the maximum of their peak values. Moreover, these quantities are plotted only for signal frequencies above the degenerate frequency $(1/2)\omega_p$ by virtue of the fact that $\Phi_{0,1,\sigma_i,\sigma_s}(-\omega_s) = \Phi_{1,0,\sigma_s,\sigma_i}(\omega_s)$.

This particular state requires that: 1) the pump mode be odd so that the spatial overlap integral does not vanish; and that 2) the phase matching conditions of the two possibilities at the preselected frequencies $\overline{\omega}_s$ and $\overline{\omega}_i$ be satisfied, i.e.,

$$\Delta\beta_{0,1,\sigma_s,\sigma_i}(\overline{\omega}_s) - 2\pi k/\Lambda^{(k)} = 0$$
$$\Delta\beta_{1,0,\sigma_s,\sigma_i}(\overline{\omega}_s) - 2\pi k/\Lambda^{(k)} = 0, \tag{2}$$

where $\Delta\beta_{m_s,m_i,\sigma_s,\sigma_i} = \beta_{m_p,\sigma_p}(\omega_p) - \beta_{m_s,\sigma_s}(\overline{\omega}_s) - \beta_{m_i,\sigma_i}(\overline{\omega}_i)$; $\overline{\omega}_i = \omega_p - \overline{\omega}_s$; β_{m_q,σ_q} is the propagation constant of wave q; and $\Lambda^{(k)}$ is the kth-order uniform poling period. The efficiency of the interaction decreases by a factor $1/k^2$ for the kth-order poling period with respect to the first-order one [44]. The choice of the TMW width w_1 determines the propagation constants of the interacting modes. The values of the waveguide width w_1 and poling period $\Lambda^{(k)}$ selected should ensure that these conditions are met or approximately met.

The indistinguishability between the down-converted photons is typically ascertained via a Hong–Ou–Mandel (HOM) interferometer [45], [46]. The rate $R(\tau)$ of photon coincidences at a pair of detectors placed at the two output ports of the interferometer is given by [13]

$$R(\tau) = \int_{-\infty}^{\infty} d\omega_s \Big\{ \big| \Phi_{0,1,\sigma_s,\sigma_i}(\omega_s) \big|^2 - \Phi_{0,1,\sigma_s,\sigma_i}(\omega_s)\Phi_{0,1,\sigma_s,\sigma_i}^*(-\omega_s)\exp\big[j(\omega_p - 2\omega_s)\tau \big] \Big\} \tag{3}$$

where τ is the temporal delay between the down-converted photons, and the asterisk denotes complex conjugation.

All of the simulations presented in this paper refer to structures that make use of Ti:LiNbO$_3$ diffused channel waveguides, as illustrated in Fig. 1. These waveguides are fabricated by diffusing a thin film of titanium (Ti), with thickness $\delta = 100$ nm and width w, into a z-cut, y-propagating LiNbO$_3$ crystal. The diffusion length D is taken to be the same in the two transverse directions: $D = 3$ μm. The TE mode polarized in the x-direction sees the ordinary refractive index n_o, whereas the TM mode polarized in the z-direction sees the extraordinary refractive index n_e.

The ordinary and extraordinary refractive indexes may be calculated by making use of the Sellmeier equations [34, ch. 5], [47], [48]. The refractive-index increase introduced by Ti indiffusion is characterized by $\Delta n = 2\delta\rho\,\text{erf}(w/2D)/\sqrt{\pi}D$, where $\rho = 0.47$ and 0.625 for n_o and n_e, respectively [49]. To accommodate wavelength dispersion, Δn can be modified by incorporating the weak factor $\xi = 0.052 + 0.065/\lambda^2$, where the wavelength λ is specified in μm [50]. We calculate the effective refractive index n_{eff} of a confined mode in two ways: 1) by using the effective-index
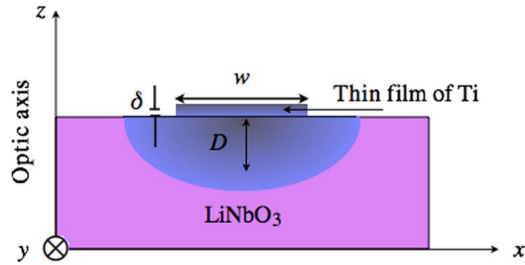
Fig. 1. Cross-sectional view of the fabrication of a diffused channel Ti:LiNbO$_3$ waveguide (not to scale). A thin film of titanium of thickness $\delta = 100$ nm and width w is diffused into a z-cut, y-propagating LiNbO$_3$ crystal. The diffusion length $D = 3$ μm.

method described in [51]; and 2) by making use of the commercial photonic and network design software package RSoft. The propagation constant of a guided mode is related to n_{eff} via $\beta = 2\pi n_{\text{eff}}/\lambda$.

In the following sections, we consider several photonic circuits for the generation, separation, and control of down-converted photons. In Section 3, we consider a circuit that generates degenerate photons in separated SMWs. In this case, the two conditions specified in (2) collapse to a single condition since $\overline{\omega}_s = \overline{\omega}_i$ and $\sigma_s = \sigma_i$. In Section 4, with a change of parameters, this same circuit is used to produce nondegenerate photons entangled in frequency or simultaneously entangled in frequency and polarization. Section 5 relates to photonic circuitry that produces nondegenerate photons distinguished by their frequencies, which leads to modal as well as modal and polarization double entanglement.

3. Photonic Circuits for Generating Degenerate Photons in Different Modes

This section is dedicated to examining the operation of a photonic circuit that produces a pair of down-converted photons and then uses their differing spatial properties (mode numbers) to ultimately guide them into two separate SMWs. The output provides a pair of degenerate photons that have even parity and can be fed into an HOM interferometer [45], [46] integrated on the same chip (see Section 6).

In particular, we consider the implementation of degenerate Type-0 (e, e, e) SPDC in a TMW of width w_1, wherein a pump photon with $m_p = 1$ is split into a pair of down-converted photons with different spatial parities. The associated two-photon state is

$$|\Psi\rangle \sim \int d\omega_s \big[\Phi_{0,1,e,e}(\omega_s)|\omega_s, e\rangle_0 |\omega_p - \omega_s, e\rangle_1 + \Phi_{1,0,e,e}(\omega_s)|\omega_s, e\rangle_1 |\omega_p - \omega_s, e\rangle_0\big] \qquad (4)$$

where the two terms merge for the degenerate case, i.e., when $\omega_s = (1/2)\omega_p$. Fig. 2(a) represents a photonic circuit that can be used to generate photon pairs of this type. The circuit comprises three sequential stages: a periodically poled region, an odd-mode coupler, and an even-mode coupler. We consider these three stages in turn.

The *periodically poled stage* shown in Fig. 2(b) is characterized by its width w_1, length L_1, and kth-order poling period $\Lambda^{(k)}$. For certain values of the width, there will always be a single value of the poling period that satisfies (2) so that there is flexibility in choosing the TMW width w_1. Once the width is assigned, the poling period is determined via (2). There are no restrictions on the length of the nonlinear stage L_1, save those associated with the process of fabrication. Increasing L_1 does, of course, increase the flux of photon pairs, but we will see in the next section that there is a limitation on how large L_1 can be made for generating entangled photons.

The *odd-mode coupler* is used to extract only the down-converted photon with an odd spatial distribution. Its principle of operation is based on selective coupling between adjacent waveguides of different widths. The even and odd modes of the TMW are characterized by different propagation constants. As depicted in Fig. 2(c), an auxiliary SMW with appropriate width w_2, length L_2, and
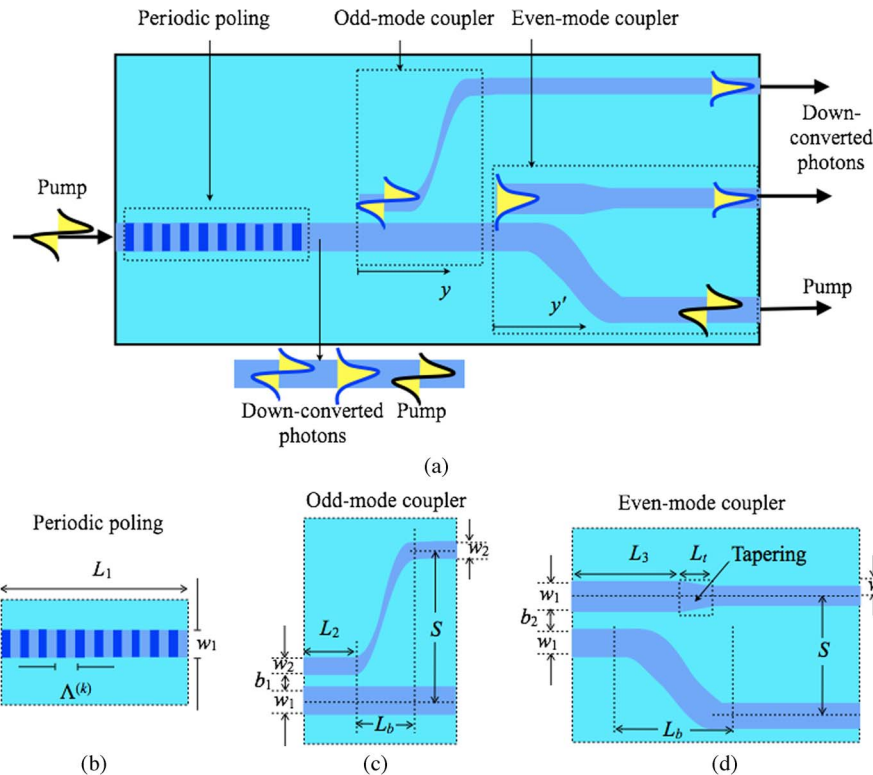
Fig. 2. (a) Sketch of a photonic circuit that can be used to generate two photons in different single-mode waveguides (not to scale). The circuit comprises three sequential stages: a periodically poled region, an odd-mode coupler, and an even-mode coupler. The parameters associated with these stages are defined in panels (b), (c), and (d), respectively. (b) The periodically poled waveguide has width w_1, length L_1, and a kth-order poling period $\Lambda^{(k)}$. (c) The odd-mode coupler is implemented by bringing a single-mode waveguide (SMW) of width w_2 and length L_2 into proximity with a two-mode waveguide (TMW) of width w_1. The two waveguides are separated by a distance b_1. An S-bend waveguide of initial and final width w_2 and bending length L_b is attached to the end of the SMW. The center-to-center separation between the output of the S-bend and the TMW is denoted S. All S-bends considered in this paper have dimensions $L_b = 10$ mm and $S = 127$ μm (the standard spatial separation [41]). (d) The even-mode coupler is implemented by bringing a second TMW of width w_1 and length L_3 into proximity with the original TMW. The two waveguides are separated by a distance b_2. The end of this second TMW is adiabatically tapered over a length L_t so that it matches the width w_2 at the output of the odd-mode coupler. The length of the taper $L_t = 1.5$ mm, as it is throughout this paper.

separation distance b_1 from the TMW can be used to phase-match the odd-mode in the TMW to the even-mode in the SMW. An S-bend waveguide in which the initial and final widths are both w_2 is attached to the end of the SMW; this obviates the possibility of further unwanted coupling to the TMW. In short, the odd-mode coupler distinguishes between the two down-converted photons based on their spatial profiles and delivers the initially odd-mode photon as an even-mode photon at its output.

The *even-mode coupler* is used to separate the down-converted photon with an even spatial profile from the pump wave. The principle of operation is based on the limited extent of the short-wavelength evanescent pump field, which precludes it from coupling to other waveguides of the same width located at typical distances. The result is that the even-mode down-converted photon alone is coupled into a second identical TMW, of length L_3 and separation distance b_2 from the original TMW, as shown in Fig. 2(d). The end of the second TMW is then coupled to an SMW of width w_2 via an adiabatically tapered waveguide region of length L_t. The tapering offers two benefits: 1) The even mode of the TMW is transformed into an even mode that matches that of the partner photon at the output of the odd-mode coupler; and 2) unwanted odd modes inadvertently coupled in from external radiation are eliminated. The down-converted degenerate photons
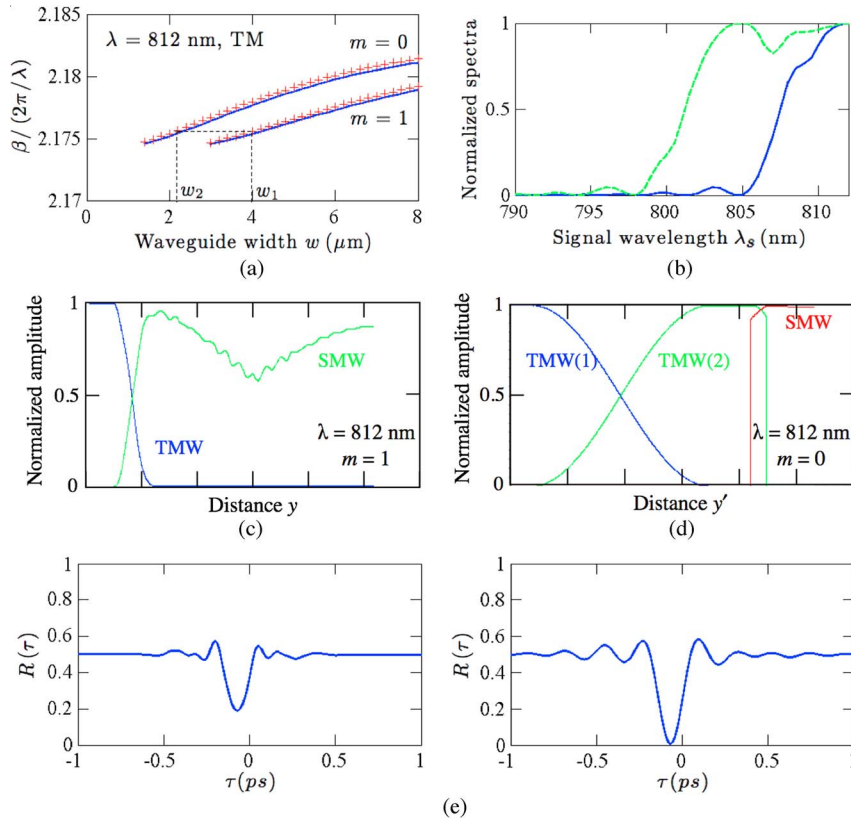
Fig. 3. Simulated performance of the photonic circuit presented in Fig. 2. A pump at wavelength $\lambda_p = 406$ nm and in an odd spatial mode ($m_p = 1$) is used to produce degenerate Type-0 (e, e, e) down-conversion with an effective nonlinear optical coefficient $d_{\text{eff}} = d_{33}$ [53]. The circuit dimensions are $w_1 = 4$ μm, $w_2 = 2.2$ μm, $L_1 = 20$ mm, $L_2 = 0.85$ mm, $L_3 = 21$ mm, and $b_1 = b_2 = 5$ μm. The poling period $\Lambda^{(1)} = 2.644$ μm is designed for operation at a temperature of 80 °C and can be temperature tuned. Values for L_b, L_t, and S are specified in the caption of Fig. 2. (a) Dependencies of the propagation constants β of the two modes for the down-converted photons on the waveguide widths w. The solid curves were obtained using the effective-index method described in [51], whereas the plus signs were computed using the software package RSoft. The dotted vertical lines represent the widths w_1 and w_2 that were chosen. (b) Dependence of the normalized output spectra on the wavelength of the signal λ_s. The solid blue and dotted green curves represent $|\Phi_{0,1,e,e}|^2$ and $|\Phi_{1,0,e,e}|^2$, respectively, for wavelengths below the degenerate value of 812 nm. (c) Performance of the odd-mode coupler. The blue and green curves represent the evolution with distance of the normalized amplitudes of the odd mode in the TMW and the even mode in the SMW, respectively. (d) Performance of the even-mode coupler. The blue, green, and red curves represent the evolution with distance of the normalized amplitudes of the even modes in the original two-mode waveguide TMW(1), in the second two-mode waveguide TMW(2), and in the SMW, respectively. The even mode of TMW(2) is defined as extending to the end of the tapered region, whereas that for the SMW is defined as initiating at the beginning of the tapered region. (e) Dependencies of the normalized coincidence rate R on the temporal delay τ, without insertion (left curve), and with insertion (right curve), of two 10-nm narrowband filters centered about 812 nm, before the two output detectors.

produced by this photonic circuit have the same mode number at the output and can therefore interfere quantum mechanically [46]. It is worthy of mention that heralded single-photon pure states in well-defined spatiotemporal modes are required for many quantum information technology applications, such as quantum cryptography [52] and linear optical quantum computing [16].

Fig. 3 provides an example in which the performance of this photonic circuit is simulated. Fig. 3(a) displays the dependencies of the fundamental and first-order mode propagation constants β on the waveguide widths w. These curves are used to select the widths of the TMW and SMW; the horizontal dotted line represents the loci of the phase-matching conditions between even and odd modes in waveguides of different widths. Fig. 3(b) shows the normalized output spectra $|\Phi_{0,1,e,e}|^2$ and $|\Phi_{1,0,e,e}|^2$ as a function of the signal wavelength λ_s. As a consequence of the large phase

mismatch between the interacting modes, the value for the first-order poling period turns out to be small, but values in this range have been realized using the method of surface poling in diffused channel waveguides [35]. Using a pump source of longer wavelength, such as 532 nm, would permit regular poling techniques to be used. A salutary feature is that the Type-0 interaction makes use of the strongest nonlinear component of the second-order tensor d_{33} so that high efficiency is expected from this interaction [53]. Figs. 3(c) and (d) display the evolution with distance of the normalized amplitudes of the interacting modes in the odd- and even-mode couplers, respectively. For the odd-mode coupler, the amplitude of the even excited mode in the SMW exhibits a dip that is associated with the tapered nature of the S-bend. The values $m = 1$ and 0 in Figs. 3(c) and (d), respectively, refer to the mode numbers at the point of generation. Fig. 3(e) displays the dependencies of the normalized coincidence rate R on the temporal delay τ, without insertion (left curve), and with insertion (right curve), of two narrowband filters at the degenerate frequency before the two output detectors. The reasons underlying the reduced visibility of the dip, and its displacement from $\tau = 0$, are considered in [13, Sec. V].

4. Photonic Circuits for Generating Spectral and Spectral/Polarization Entanglement

Changing the values of the parameters provided in Fig. 3 allows the circuit shown in Fig. 2 to produce two nondegenerate down-converted photons that are entangled in frequency, or simultaneously in frequency and polarization, via a Type-0 or Type-II interaction, respectively.

Using the mode numbers to distinguish the photons, (1) takes the form

$$|\Psi\rangle \sim \int d\omega_s \big[\Phi_{0,1,\sigma_s,\sigma_i}(\omega_s)|\omega_s, \sigma_s\rangle_0 |\omega_i, \sigma_i\rangle_1 + \Phi_{1,0,\sigma_s,\sigma_i}(\omega_s)|\omega_s, \sigma_s\rangle_1 |\omega_i, \sigma_i\rangle_0\big]. \tag{5}$$

However, some restrictions apply to the generation and separation portions of the circuit, as discussed in the following paragraphs.

With respect to the generation region, values of the waveguide width w and poling period $\Lambda^{(k)}$ govern how the conditions in (2) are satisfied. Simulations show that: 1) for certain values of the waveguide width, slightly different poling periods are required to satisfy these conditions; and 2) the absolute difference between the quantities $[\beta_{0,\sigma_s}(\overline{\omega}_s) + \beta_{1,\sigma_i}(\overline{\omega}_i)]$ and $[\beta_{0,\sigma_i}(\overline{\omega}_i) + \beta_{1,\sigma_s}(\overline{\omega}_s)]$, which appear in (2), is *nearly* independent of waveguide width. Consequently, the choice of w_1 can be left to other considerations, such as fabrication limitations and subsequent design requirements.

Our strategy is to satisfy the sum condition, rather than each condition individually, for a specified value of the waveguide width, so that

$$\Delta\beta_{\text{avg}}(\overline{\omega}_s) - 2\pi k/\Lambda^{(k)} = 0, \tag{6}$$

where $\Delta\beta_{\text{avg}} = (1/2)[\Delta\beta_{0,1,\sigma_s,\sigma_i}(\overline{\omega}_s) + \Delta\beta_{1,0,\sigma_s,\sigma_i}(\overline{\omega}_s)]$. Substituting the value of the poling period $\Lambda^{(k)}$ obtained in both conditions of (2) leads to small errors in satisfying the phase-matching conditions for the two interactions. These errors can be used to determine the coherence lengths for the two interactions, which then provide upper bounds to the length of the periodically poled region L_1. The choice of L_1 must also result in good spectral overlap between $|\Phi_{0,1,\sigma_s,\sigma_i}(\omega_s)|^2$ and $|\Phi_{1,0,\sigma_s,\sigma_i}(\omega_s)|^2$ around the preselected frequencies, since L_1 determines the widths of these functions. It turns out that this strategy leads to almost maximally entangled states at the preselected frequencies.

With respect to the coupling region, the design must optimize coupling at both preselected frequencies, $\overline{\omega}_s$ and $\overline{\omega}_i$. The choice of w_1 and w_2 for the odd-mode coupler is based on satisfying the phase matching conditions between an odd mode in a TMW of width w_1 and an even mode in a SMW of width w_2, for both $\overline{\omega}_s$ and $\overline{\omega}_i$:

$$\beta_{1,\sigma_s}(\overline{\omega}_s, w_1) = \beta_{0,\sigma_s}(\overline{\omega}_s, w_2)$$
$$\beta_{1,\sigma_i}(\overline{\omega}_i, w_1) = \beta_{0,\sigma_i}(\overline{\omega}_i, w_2). \tag{7}$$

Since the down-conversion generation process depends only weakly on waveguide width, we select the TMW width in the generation region to be equal to w_1; this obviates the need to taper the waveguide from the periodically poled region to the odd-mode coupler. The coupling length is frequency and polarization dependent, however, so that the SMW length L_2, in combination with the separation distance b_1, must be carefully chosen to maximize the coupling for both $\overline{\omega}_s$ and $\overline{\omega}_i$. The same considerations apply for the even-mode coupler so that the second TMW length L_3 and separation distance b_2 are selected similarly.

An example, provided in Fig. 4, illustrates the simulated performance of the photonic circuit shown in Fig. 2 to generate spectrally entangled photons. Consider nondegenerate Type-0 (e, e, e) SPDC, in which a pump laser of wavelength 406 nm, in mode $m_p = 1$, generates two photons centered about the wavelengths 780 nm and 846.7 nm. The TMW width w_1 and the SMW width w_2 are determined via Fig. 4(a), which represents the dependencies of the propagation constants on waveguide width. The values w_1 and w_2 are chosen to satisfy (7) as closely as possible. Fig. 4(b) displays the output normalized spectra, $|\Phi_{0,1,e,e}(\omega_s)|^2$ and $|\Phi_{1,0,e,e}(\omega_s)|^2$, for an SPDC poling length L_1 that was selected to attain maximum entanglement and high efficiency. The performance of the odd- and even-mode couplers are displayed in Figs. 4(c) and (d), respectively; each panel contains plots for the two frequencies $\overline{\omega}_s$ and $\overline{\omega}_i$. The values $m = 1$ and 0 in Figs. 4(c) and (d), respectively, refer to the mode numbers at the point of generation, and the curves are color-coded in the same way as the corresponding curves in Fig. 3. The values of L_2 (L_3) and b_1 (b_2) are selected to optimize coupling of the odd (even) modes for both $\overline{\omega}_s$ and $\overline{\omega}_i$. Fig. 4(e) displays the behavior of the normalized coincidence rate function $R(\tau)$ for the down-converted photons, without insertion (left curve), and with insertion (right curve), of two 10-nm narrowband filters, centered about 780 and 846. 7 nm, before the two output detectors.

An example based on nondegenerate Type-II (o, e, o) SPDC, which is illustrated in Fig. 5, suggests that simultaneous spectral and polarization entanglement can be obtained by again making use of the photonic circuit shown in Fig. 2. By convention, the notation $(\cdot, \cdot, \cdot)$ indicates, in consecutive order, the polarization of the down-converted photon whose frequency lies above the degenerate frequency, the down-converted photon whose frequency lies below the degenerate frequency, and the pump photon. Type-II behavior is obtained by using a TE pump in place of the TM pump employed in Fig. 4 and by choosing the circuit-element parameters, including $\Lambda^{(k)}$, appropriately. The panels displayed in Fig. 5 are similar to those shown in Fig. 4. Again, the values $m = 1$ and 0 in Figs. 5(c) and (d), respectively, refer to the mode numbers at the point of generation, and the curves are color-coded in the same way as the corresponding curves in Figs. 3 and 4. In principle, spectral and polarization double entanglement [13] could also be attained with this arrangement, but the parameters that achieve it are not easily established.

5. Photonic Circuits for Generating Modal and Double Modal/Polarization Entanglement

This section focuses on the operation of a photonic circuit that generates modal entanglement by distinguishing two nondegenerate photons on the basis of their frequencies, rather than their mode numbers. Modally entangled photons in a TMW have the following property: A photon whose frequency lies above the degenerate frequency and appears in the fundamental (even) mode is always accompanied by another whose frequency lies below the degenerate frequency and appears in the first-order (odd) mode, and *vice versa*. Alternatively, the photons could be distinguished on the basis of their polarizations in the context of a Type-II configuration. When the photons are distinguished on the basis of their frequencies, the biphoton state (1) is written as

$$|\Psi\rangle \sim \int d\omega_s \left[\Phi_{0,1,\sigma_s,\sigma_i}(\omega_s)|0, \sigma_s\rangle_{\omega_s}|1, \sigma_i\rangle_{\omega_i} + \Phi_{1,0,\sigma_s,\sigma_i}(\omega_s)|1, \sigma_s\rangle_{\omega_s}|0, \sigma_i\rangle_{\omega_i} \right]. \qquad (8)$$

Modal entanglement is generated by the photonic circuit displayed in Fig. 6. It comprises three stages. The first *periodically poled stage* is a nonlinear region, as in Fig. 2(b), that produces a pair of
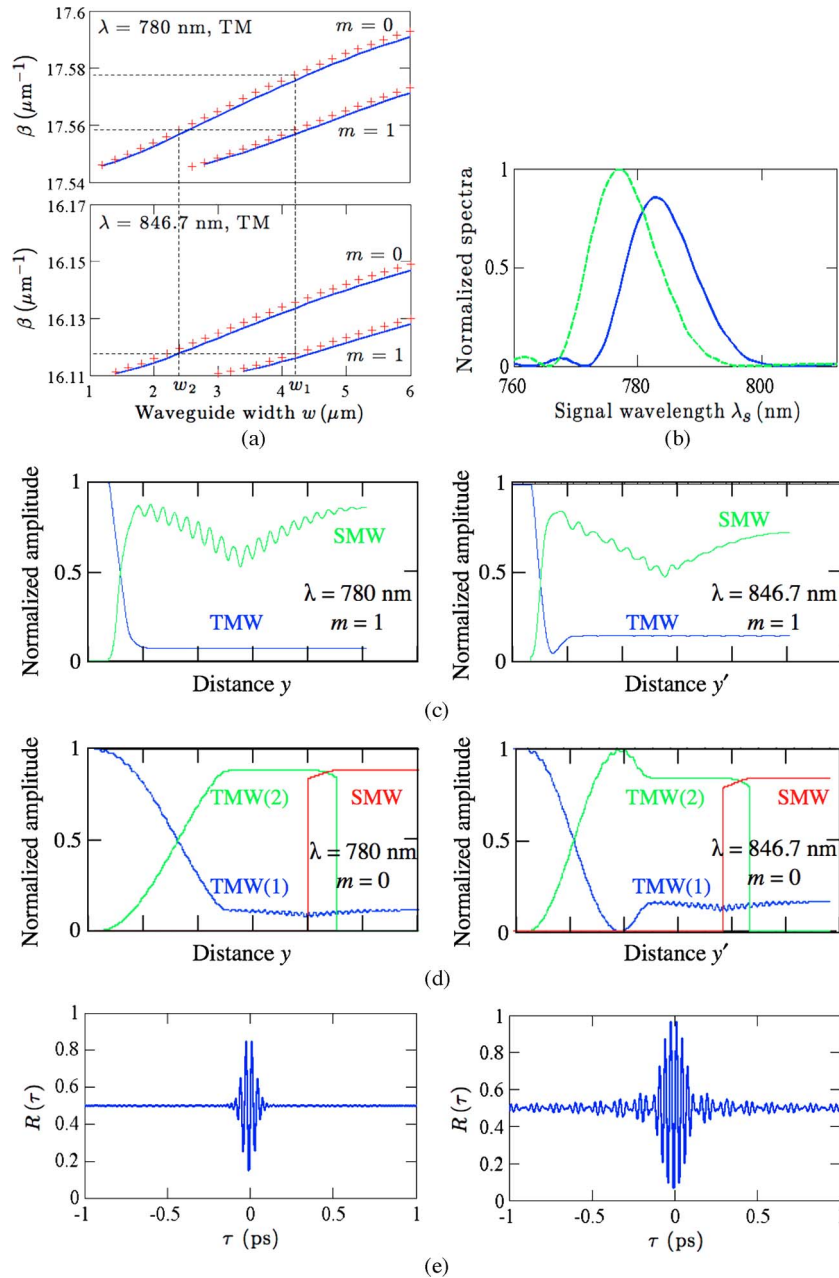
Fig. 4. Simulated performance of the photonic circuit portrayed in Fig. 2 when configured to generate spectrally entangled photons. An odd-mode ($m_p = 1$) TM laser pump at $\lambda_p = 406$ nm is used to generate nondegenerate Type-0 (e, e, e) SPDC with a nonlinear optical coefficient $d_{\text{eff}} = d_{33}$. The center wavelengths of the two down-converted photons are 780 nm and 846.7 nm. The circuit dimensions are $w_1 = 4.2$ μm, $w_2 = 2.4$ μm, $L_1 = 2$ mm, $L_2 = 0.18$ mm, $L_3 = 11$ mm, and $b_1 = b_2 = 4$ μm. The poling period $\Lambda^{(1)} = 2.588$ μm is designed for operation at a temperature of 80 °C and can be temperature tuned. The panels in this figure are similar to those displayed in Fig. 3, except that panels (a), (c), and (d) each contain separate plots for the two wavelengths. Furthermore, in panel (e), the two filters placed in front of the detectors are centered about 780 nm and 846.7 nm, instead of both being centered about 812 nm, as for degenerate down-conversion.

nondegenerate down-converted photons via SPDC. As discussed in Section 3, this stage is characterized by its width w_1, length L_1, and kth-order poling period $\Lambda^{(k)}$. The choice of these parameters is governed by the same considerations as those attendant to the discussion in Section 4.
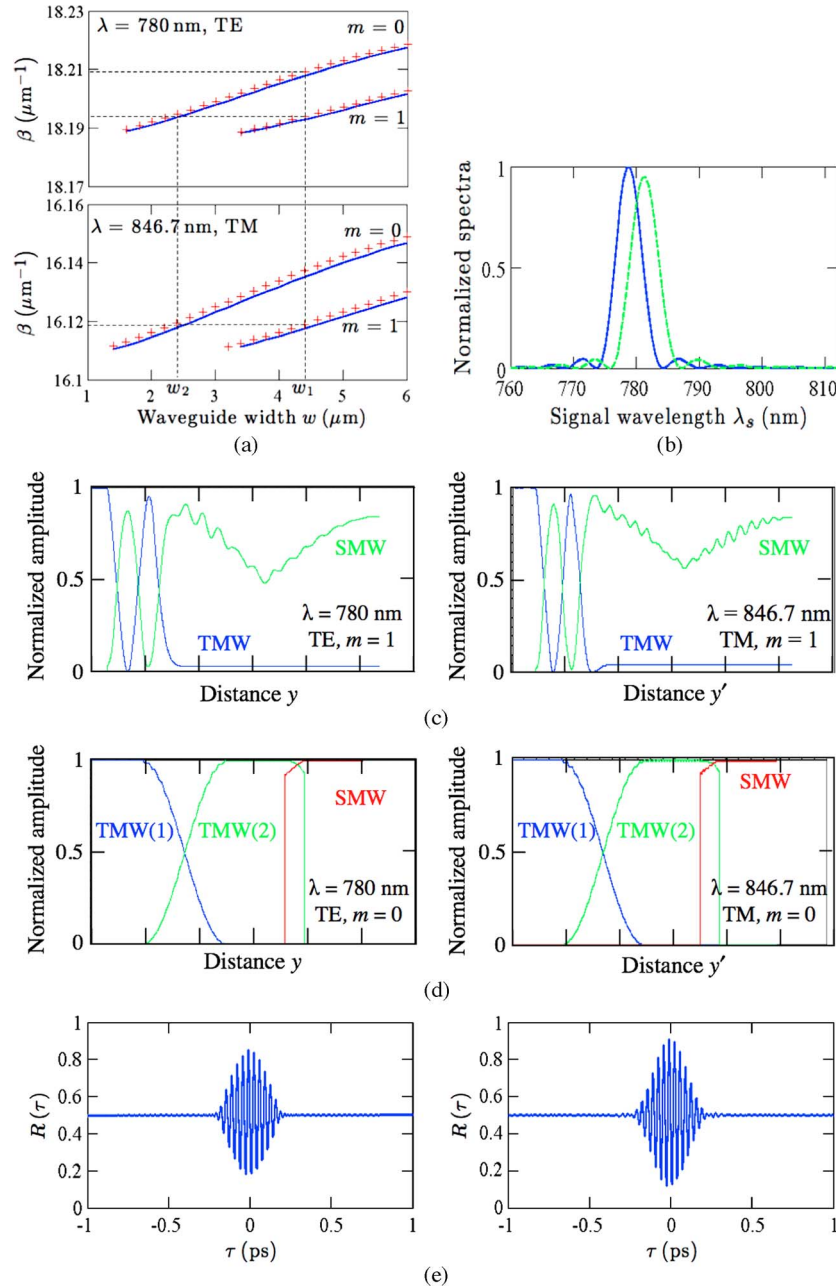
Fig. 5. Simulated performance of the photonic circuit displayed in Fig. 2 when configured to generate photons simultaneously entangled in frequency and polarization. A laser pump at $\lambda_p = 406$ nm, in mode $m_p = 1$, is used to produce nondegenerate Type-II (o, e, o) SPDC, with a nonlinear optical coefficient $d_{\text{eff}} = d_{31} \ll d_{33}$ [53]. A TE pump is used in place of the TM pump employed in Fig. 4, and $\Lambda^{(k)}$ is chosen appropriately. The center wavelengths of the two down-converted photons are 780 nm and 846.7 nm. The circuit dimensions are $w_1 = 4.4$ μm, $w_2 = 2.4$ μm, $L_1 = 1$ mm, $L_2 = 1.95$ mm, $L_3 = 11$ mm, and $b_1 = b_2 = 4$ μm. The poling period $\Lambda^{(1)} = 1.869$ μm is designed for operation at a temperature of 80 °C and can be temperature tuned. All panels are similar to those displayed in Fig. 4 for nondegenerate Type-0 (e, e, e) SPDC.

The second stage is a *holographic Bragg grating* that distinguishes the down-converted photons based on their frequencies, such as by reflecting the low-frequency photon while transmitting the high-frequency photon so that they travel in opposite directions. The third stage consists of two couplers that transfer the even and odd down-converted photons from the original waveguide in
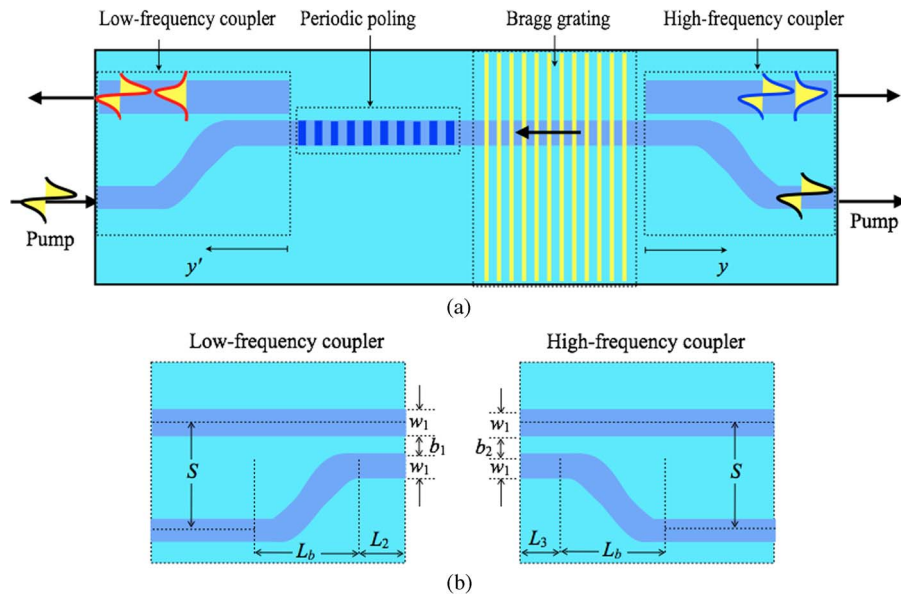
Fig. 6. (a) Sketch of a photonic circuit that can be used to generate two photons entangled in mode number (not to scale). The circuit comprises three stages: a periodically poled region, a holographic Bragg grating, and two couplers (a low-frequency coupler located to the left and a high-frequency coupler located to the right). The periodically poled waveguide is identical to that portrayed in Fig. 2(b), with width w_1, length L_1, and poling period $\Lambda^{(k)}$. The holographic Bragg grating reflects the low-frequency photon and transmits the high-frequency photon. (b) Definitions of the parameters associated with the couplers. As in Fig. 2(c), $L_b = 10$ mm and $S = 127$ μm.

which they are generated to the output-port waveguides of the circuit, via a *low-frequency coupler* to the left and a *high-frequency coupler* to the right.

The holographic Bragg grating can be inscribed on the Ti:LiNbO$_3$ waveguide by superposing two coherent plane waves and making use of proton exchange [54] or a dopant such as Cu together with thermal fixing [39]. The sinusoidal light-intensity pattern generated by the superposition of the plane waves [34, ch. 2] is impressed on the waveguide as a sinusoidal modulation of the refractive index. The wavelength of light at which the reflected intensity is maximum (for normal incidence) is $\lambda = 2n_{\text{eff}} \Lambda_B$, where Λ_B is the grating period, and n_{eff} is the effective refractive index of the guided mode. The bandwidth of the reflected light decreases with increasing grating length. The fundamental and first-order modes can be reflected at a given wavelength by making use of either a single hologram of short length or two multiplexed holograms of longer length. Multiplexing is most effectively achieved by recording the holograms sequentially [39].

The low- and high-frequency couplers are designed to couple the idler-frequency ($\overline{\omega}_i$) and signal-frequency ($\overline{\omega}_s$) photons, respectively, into separate output TMWs that exclude the pump, as shown in Fig. 6. This is achieved by bringing two auxiliary TMWs into proximity with the principal TMW; all are of the same width w_1; therefore, the spatial profiles of both the even and odd modes can be maintained in the course of coupling. The pump fails to couple to these auxiliary TMWs because it has a short-range evanescent field by virtue of its high frequency. The lengths of the auxiliary TMWs and their separation distances are designed to optimize coupling of both the even and the odd modes. For the low-frequency (high-frequency) coupler, the auxiliary TMW is of length L_2 (L_3), and the separation distance is b_1 (b_2) from the principal waveguide, as illustrated in Fig. 6(b).

A simulation in which the photonic circuit in Fig. 6 is used to generate a pair of photons entangled in mode number is presented in Fig. 7. The nonlinear SPDC source is identical to that displayed in Fig. 4. The Bragg grating consists of two multiplexed holograms, with periods of 83.8 and 83.7 nm, to reflect the fundamental and first-order modes of the low-frequency down-converted photon, respectively. Figs. 7(a) and (b) displays the performance of the low- and
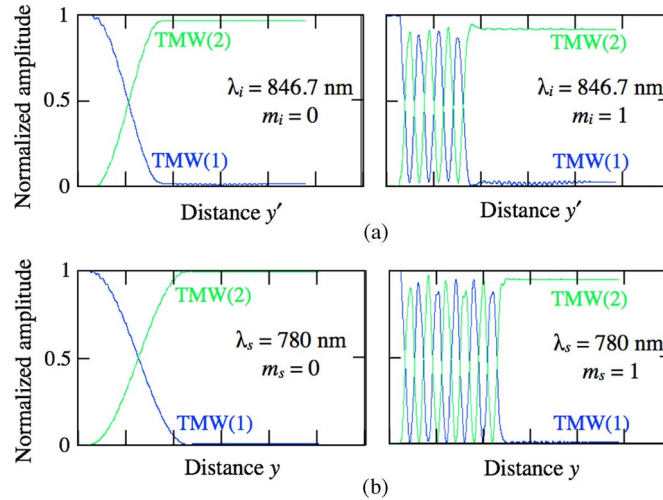
Fig. 7. Simulated performance of the photonic circuit described in Fig. 6 for generating photons entangled in mode number. The Type-0 (e, e, e) SPDC source is identical to that used in Fig. 4; nondegenerate photon pairs with center wavelengths of 846.7 nm and 780 nm are generated using a poling period of $\Lambda^{(1)} = 2.588$ μm. The circuit dimensions are $w_1 = 4.2$ μm, $L_1 = 2$ mm, $L_2 = 4.1$ mm, $L_3 = 8.25$ mm, and $b_1 = b_2 = 4$ μm. The Bragg grating comprises two multiplexed holograms, with periods of 83.8 and 83.7 nm, so that both the even and odd modes associated with the low-frequency photon can be reflected. (a) and (b) Performance of the low-and high-frequency couplers, respectively. Each panel contains separate plots for the fundamental $(m = 0)$ and first-order $(m = 1)$ modes. For the left (right) subplots, the blue and green curves represent the evolution with distance of the normalized even (odd) modes in the original and auxiliary TMWs, respectively.

high-frequency couplers, respectively. Each panel has two subplots, for the even $(m = 0)$ and odd modes $(m = 1)$. For both frequencies, the coupling length of the first-order mode is substantially shorter than that of the fundamental mode since the peaks of the field for the former lie closer to the transverse edges of the waveguide. Since the coupling length is fixed, multiple cycles of energy transfer of the odd modes (right panels) are required to assure full coupling of the even modes (left panels).

A modified version of the photonic circuit displayed in Fig. 6 can also be used to generate photons, via a Type-II interaction, that are doubly entangled in mode number and polarization. The biphoton state in that case is

$$|\Psi\rangle \sim \int d\omega_s \Big[\Phi_{0,1,o,e}(\omega_s)|0, o\rangle_{\omega_s}|1, e\rangle_{\omega_i} + \Phi_{1,0,o,e}(\omega_s)|1, o\rangle_{\omega_s}|0, e\rangle_{\omega_i}$$

$$+ \Phi_{0,1,e,o}(\omega_s)|0, e\rangle_{\omega_s}|1, o\rangle_{\omega_i} + \Phi_{1,0,e,o}(\omega_s)|1, e\rangle_{\omega_s}|0, o\rangle_{\omega_i} \Big]. \quad (9)$$

This interaction can be viewed as a superposition of Type-II (o, e, o) and Type-II (e, o, o). To generate such doubly entangled photons, the periodically poled nonlinear region portrayed in Fig. 6 would have to be replaced by nonuniform (e.g., linearly chirped) poling, or aperiodic poling [55], to satisfy the phase matching conditions for the four possibilities. Also, the holographic Bragg grating would then have to consist of four multiplexed holograms of long length or two multiplexed holograms of short length. Since the Bragg-grating outputs in both directions could be a photon in the fundamental- or first-order mode, with transverse-electric or transverse-magnetic polarization, the low- and high-frequency couplers would both have to be designed to optimize coupling for all of the possibilities. It is worthy to mention that states entangled in more than one degree of freedom are the primary resource for one-way computation [15].

An example to illustrate the simulated performance of such a photonic circuit for generating photons that are doubly entangled in mode number and polarization is displayed in Fig. 8. As shown in Fig. 8(a), the use of linearly chirped poling leads to broadband spectra. The low-frequency photon would be filtered using the Bragg grating, while the high-frequency photon could be filtered
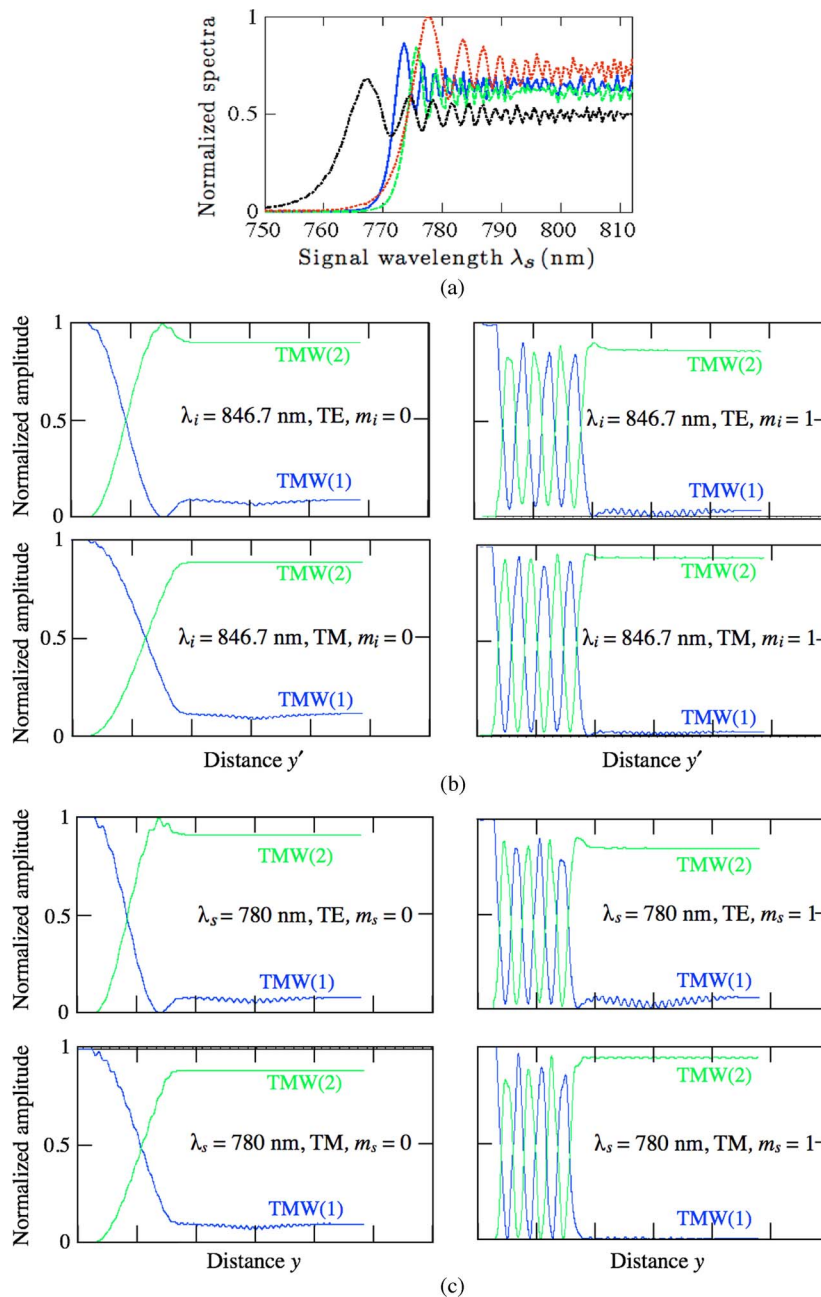
Fig. 8. Simulated performance of a modified version of the photonic circuit displayed in Fig. 6 for generating photons that are doubly entangled in mode number and polarization. An o-polarized pump at $\lambda_p = 406$ nm, and in mode $m_p = 1$, is used to produce nondegenerate photons via Type-II (o, e, o) and (e, o, o) SPDC processes. The preselected center wavelengths of the down-converted photons are again 846.7 nm and 780 nm. The periodically poled region is linearly chirped over a distance $L_1 = 20$ mm with an initial poling period of 1.84 μm and a final poling period of 1.87 μm. The Bragg grating comprises four multiplexed holograms, with periods 83.7, 83.8, 80.8 and 80.9 nm, designed to reflect the low-frequency photons in the backward direction. Other circuit dimensions are $w_1 = 4.4$ μm, $L_2 = 4.6$ mm, $L_3 = 3.8$ mm, $b_1 = 4$ μm, and $b_2 = 3.5$ μm. (a) Normalized spectra at the output of the nonlinear region versus the signal wavelength λ_s. The solid blue and dashed green curves represent the output spectra associated with Type-II (o, e, o) SPDC, whereas the dash-dotted black and dotted red curves represent the output spectra associated with Type-II (e, o, o) SPDC. (b) and (c) Performance of the low- and high-frequency couplers, respectively. Each of these panels contains four subplots: The top (bottom) subplots represent TE (TM) polarization, while the left (right) subplots represent the fundamental (first-order) mode. The blue and green curves represent the evolution with distance of the normalized modes in the original and auxiliary TMWs, respectively.

by placing a narrowband filter at the output detector. The generation of narrowband spectra could, in principle, be achieved by making use of aperiodic poling; however, this would require poling periods so small that they might be beyond the capabilities of current fabrication techniques.

6. Photonic Circuits for Dispersion Management

The presence of dispersion is deleterious to the operation of photonic circuits used for many quantum-information applications. Dispersion results from the dependence of the propagation constant β on frequency, mode number, and polarization. Polarization-mode dispersion generally provides the strongest contribution, especially in a birefringent material such as LiNbO$_3$. However, the Type-0 (e, e, e) interaction, by virtue of its three parallel electric field vectors, suffers only from frequency and modal dispersion, and these are often sufficiently weak that they can be neglected for short devices. This is not the case for Type-II circuits, however, where polarization-mode dispersion is indeed dominant.

In this section, we address the management of dispersion and consider possible ways of mitigating it in photonic circuits, whatever the type of interaction. The optimal approach for circumventing dispersion depends on the particular application.

An example that proves instructive is the photonic-circuit HOM interferometer, in which a simple adjustment of the path length can be effective. The photonic circuit shown in Fig. 2 provides for the generation, separation, and guidance of two SPDC photons into two distinct SMW output ports. An HOM interferometer can be fabricated on the same chip by feeding these outputs into a 3-dB coupler endowed with an electrooptic phase modulator in one of its input arms. This allows a variable phase delay to be introduced between the photons, thereby enabling an interferogram to be generated.

The presence of dispersion alters the coincidence rate $R(\tau)$ associated with the HOM interferometer. The origin of this effect can be understood by casting the interferometer as a four-port system with each arm behaving as an ideal phase filter. Referring to Fig. 2, the matrix $\mathbf{T}$ that relates the output and input of the system then takes the form

$$\mathbf{T} = \begin{bmatrix} H(\omega) & 0 \\ 0 & H(\omega) \end{bmatrix} \begin{bmatrix} 1 & j \\ j & 1 \end{bmatrix} \begin{bmatrix} H(\omega)H_o(\omega) & 0 \\ 0 & H(\omega)H_e(\omega) \end{bmatrix} \tag{10}$$

with

$$\begin{aligned} H(\omega) &= \exp\left[-j\beta_{1,\sigma}(\omega)\, l\right] \\ H_o(\omega) &= \exp\left[-j\beta_{1,\sigma}(\omega)\, l_o\right] \\ H_e(\omega) &= \exp\left[-j\beta_{1,\sigma}(\omega)\, L_t/2 - j\beta_{0,\sigma}(\omega)(l_e + L_t/2)\right] \end{aligned} \tag{11}$$

where l is the length of an arm of the 3-dB coupler; l_e and l_o are the distances traveled by the even and odd modes from the generation region to the 3-dB coupler, respectively; L_t is the length of the tapered region; and the sandwiched matrix characterizes the lossless beam splitter. The mode in the adiabatically tapered region is assumed to propagate with propagation constant $(1/2)[\beta_{0,\sigma}(\omega) + \beta_{1,\sigma}(\omega)]$.

The presence of dispersion results in a modification of the coincidence rate $R(\tau)$. In particular, the second term of (3) is modified by the quantity

$$D(\omega_s) = T_{11}^*(\omega_s)\, T_{22}^*(\omega_i)\, T_{21}(\omega_i)\, T_{12}(\omega_s) \tag{12}$$

where $\omega_i = \omega_p - \omega_s$, and the T_{uv} are elements of the $\mathbf{T}$ matrix with u and v representing row and column indexes, respectively. Substituting (10) and (11) into (12) yields

$$D(\omega_s) = \exp\left\{ j\left[\beta_{1,\sigma_s}(\omega_s) - \beta_{1,\sigma_i}(\omega_i)\right][l_o - L_t/2] - j\left[\beta_{0,\sigma_s}(\omega_s) - \beta_{0,\sigma_i}(\omega_i)\right][l_e + L_t/2] \right\} \tag{13}$$
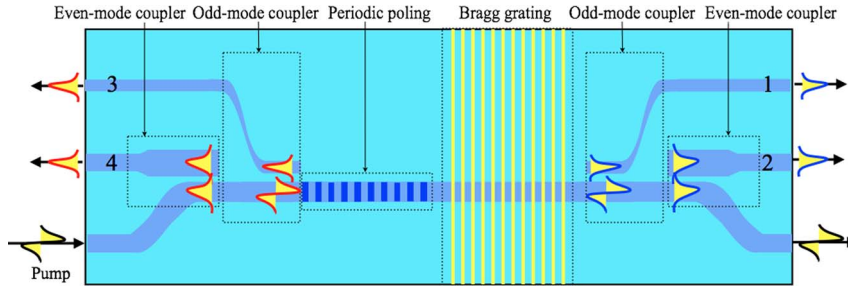
Fig. 9. Photonic circuit that generates photons entangled in path (not to scale). After generation in the nonlinear region, they are separated first on the basis of their frequencies and then on the basis of their mode numbers.

which, together with (2), gives rise to

$$D(\overline{\omega}_s) = \exp\{j[\beta_{1,\sigma_s}(\overline{\omega}_s) - \beta_{1,\sigma_i}(\overline{\omega}_i)][l_o - l_e - L_t].$$ (14)

It is apparent that choosing $l_o = l_e + L_t$ results in dispersion cancellation at the preselected frequencies. Moreover, it leads to even-order dispersion cancellation for other frequency components as well.

More generally, the deleterious effects of dispersion can be mitigated by mapping every possibility for each available degree of freedom into a different path, resulting in the conversion of modal, spectral, and polarization entanglement into path entanglement.

Consider, as an example, a Type-II (e, o, o) interaction. In this case, frequency and polarization are effectively only a single degree of freedom since the photon with frequency above (below) the degenerate value is always $e(o)$. Thus, two degrees of freedom suffice for characterizing the system: frequency or polarization and mode number. A photonic circuit for converting these two degrees of freedom into photons entangled in path is sketched in Fig. 9. The photons are first separated on the basis of their frequencies and then on the basis of their mode numbers. Each output port thus carries only a particular degree of freedom, thereby skirting the distinguishability engendered by dispersion-induced time delay. The circuit displayed in Fig. 9 can be viewed as a superposition of those illustrated in Figs. 2 and 6.

The biphoton state entangled in path can be written as

$$|\Psi\rangle \sim \int d\omega_s \big[\Phi_{0,1,\sigma_s,\sigma_i}(\omega_s)|\omega_s, 0, \sigma_s\rangle_1 |\omega_i, 1, \sigma_i\rangle_3 + \Phi_{1,0,\sigma_s,\sigma_i}(\omega_s)|\omega_s, 1, \sigma_s\rangle_2 |\omega_i, 0, \sigma_i\rangle_4\big]$$ (15)

where the subscripts 1, 2, 3, and 4 refer to the output ports labeled in Fig. 9. The photon of frequency ω_i is assumed to be back-reflected by the holographic Bragg grating.

In the case of double entanglement, each output port in a circuit such as that shown in Fig. 9 would deliver photons with either TE- or TM-polarization. To avoid distinguishability as a result of polarization-mode dispersion, two methods could be used: 1) Each output port could be split into a pair of ports, resulting in eight doubly entangled paths; or 2) an electrooptic TE$\rightleftharpoons$TM mode converter [38] could be used at the path center of each output port, thereby advancing the slow, and retarding the fast, photons in such a way that they would arrive simultaneously at the output detectors.

7. Conclusion

We have presented several photonic-circuit designs based on Ti:LiNbO$_3$ diffused channel waveguides for generating photons with various combinations of modal, spectral, and polarization entanglement. These circuits contain, in various forms, a nonlinear periodically poled TMW structure,

SMW- and TMW-based couplers, and multiplexed holographic Bragg gratings. Depending on the choice of parameters, the first photonic circuit produces frequency-degenerate down-converted photons with even spatial parity, nondegenerate down-converted photons entangled in frequency, or nondegenerate down-converted photons simultaneously entangled in frequency and polarization. The second photonic circuit produces modal entanglement or photons that are doubly entangled in mode number and polarization. The third photonic circuit converts modal, spectral, and polarization entanglement into path entanglement to mitigate the effects of dispersion. Simulations have been carried out, with the help of the commercial photonic and network design software package RSoft, to gauge the performance of these circuits. Furthermore, since Ti:LiNbO$_3$ photonic circuits have the salutary property of permitting the generation, transmission, and processing of photons to be accommodated on a single chip, we expect that they will find use in the efficient implementation of various quantum information processing schemes [14].

References

[1] A. Aspect, P. Grangier, and G. Roger, "Experimental tests of realistic local theories via Bell's theorem," *Phys. Rev. Lett.*, vol. 47, pp. 460–463, Aug. 1981.

[2] D. N. Klyshko, *Photons and Nonlinear Optics.*　　Moscow, Russia: Nauka, 1980 Translation: Gordon and Breach, New York, 1988.

[3] A. Joobeur, B. E. A. Saleh, and M. C. Teich, "Spatiotemporal coherence properties of entangled light beams generated by parametric down-conversion," *Phys. Rev. A*, vol. 50, no. 4, pp. 3349–3361, Oct. 1994.

[4] A. Joobeur, B. E. A. Saleh, T. S. Larchuk, and M. C. Teich, "Coherence properties of entangled light beams generated by parametric downconversion: Theory and experiment," *Phys. Rev. A*, vol. 53, no. 6, pp. 4360–4371, Jun. 1996.

[5] B. E. A. Saleh, A. F. Abouraddy, A. V. Sergienko, and M. C. Teich, "Duality between partial coherence and partial entanglement," *Phys. Rev. A*, vol. 62, no. 4, p. 043816, Sep. 2000.

[6] J. G. Rarity and P. R. Tapster, "Experimental violation of Bell's inequality based on phase and momentum," *Phys. Rev. Lett.*, vol. 64, no. 21, pp. 2495–2498, May 1990.

[7] J. D. Franson, "Inconsistency of local realistic descriptions of two-photon interferometer experiments," *Phys. Rev. A*, vol. 61, no. 1, p. 012105, Dec. 1999.

[8] A. Mair, A. Vaziri, G. Weihs, and A. Zeilinger, "Entanglement of the orbital angular momentum states of photons," *Nature*, vol. 412, no. 6844, pp. 313–316, Jul. 2001.

[9] S. P. Walborn, S. Pádua, and C. H. Monken, "Conservation and entanglement of Hermite–Gaussian modes in parametric down-conversion," *Phys. Rev. A*, vol. 71, no. 5, p. 053812, May 2005.

[10] A. F. Abouraddy, T. Yarnall, B. E. A. Saleh, and M. C. Teich, "Violation of Bell's inequality with continuous spatial variables," *Phys. Rev. A*, vol. 75, no. 5, p. 052114, May 2007.

[11] T. Yarnall, A. F. Abouraddy, B. E. A. Saleh, and M. C. Teich, "Experimental violation of Bell's inequality in spatial-parity space," *Phys. Rev. Lett.*, vol. 99, no. 17, p. 170408, Oct. 2007.

[12] T. Yarnall, A. F. Abouraddy, B. E. A. Saleh, and M. C. Teich, "Synthesis and analysis of entangled photonic qubits in spatial-parity space," *Phys. Rev. Lett.*, vol. 99, no. 25, p. 250502, Dec. 2007.

[13] M. F. Saleh, B. E. A. Saleh, and M. C. Teich, "Modal, spectral, and polarization entanglement in guided-wave parametric down-conversion," *Phys. Rev. A*, vol. 79, no. 5, p. 053842, May 2009.

[14] M. F. Saleh, G. Di Giuseppe, B. E. A. Saleh, and M. C. Teich, *Modal and polarization qubits in Ti:LiNbO$_3$ photonic circuits for a universal quantum logic gate.* [Online]. Available: http://arxiv.org/abs/1007.3256

[15] R. Raussendorf and H. J. Briegel, "A one-way quantum computer," *Phys. Rev. Lett.*, vol. 86, no. 22, pp. 5188–5191, May 2001.

[16] E. Knill, R. Laflamme, and G. J. Milburn, "A scheme for efficient quantum computation with linear optics," *Nature*, vol. 409, no. 6816, pp. 46–52, Jan. 2001.

[17] A. Politi, M. J. Cryan, J. G. Rarity, S. Yu, and J. L. O'Brien, "Silica-on-silicon waveguide quantum circuits," *Science*, vol. 320, no. 5876, pp. 646–649, May 2008.

[18] J. C. F. Matthews, A. Politi, A. Stefanov, and J. L. O'Brien, "Manipulation of multiphoton entanglement in waveguide quantum circuits," *Nature Photon.*, vol. 3, no. 6, pp. 346–350, Jun. 2009.

[19] C. H. Bennett and P. W. Shor, "Quantum information theory," *IEEE Trans. Inf. Theory*, vol. 44, no. 6, pp. 2724–2742, Oct. 1998.

[20] M. A. Nielsen and I. L. Chuang, *Quantum Computation and Quantum Information.*　　Cambridge, U.K.: Cambridge Univ. Press, 2000.

[21] J. L. O'Brien, A. Furusawa, and J. Vuckovic, "Photonic quantum technologies," *Nature Photon.*, vol. 3, no. 12, pp. 687–695, Dec. 2009.

[22] A. Politi, J. C. F. Matthews, M. G. Thompson, and J. L. O'Brien, "Integrated quantum photonics," *IEEE J. Sel. Topics Quantum Electron.*, vol. 15, no. 6, pp. 1673–1684, Nov./Dec. 2009.

[23] G. Cincotti, "Prospects on planar quantum computing," *J. Lightw. Technol.*, vol. 27, no. 24, pp. 5755–5766, Dec. 2009.

[24] T. D. Ladd, F. Jelezko, R. Laflamme, Y. Nakamura, C. Monroe, and J. L. O'Brien, "Quantum computers," *Nature*, vol. 464, no. 7285, pp. 45–53, Mar. 2010.

[25] M. Fiorentino, S. M. Spillane, R. G. Beausoleil, T. D. Roberts, P. Battle, and M. W. Munro, "Spontaneous parametric down-conversion in periodically poled KTP waveguides and bulk crystals," *Opt. Express*, vol. 15, no. 12, pp. 7479–7488, Jun. 2007.

[26] M. Avenhaus, M. V. Chekhova, L. A. Krivitsky, G. Leuchs, and C. Silberhorn, "Experimental verification of high spectral entanglement for pulsed parametric down-conversion," *Phys. Rev. A*, vol. 79, no. 4, p. 043836, Apr. 2009.

[27] P. J. Mosley, A. Christ, A. Eckstein, and C. Silberhorn, "Direct measurement of the spatial-spectral structure of waveguided parametric down-conversion," *Phys. Rev. Lett.*, vol. 103, no. 23, p. 233901, Dec. 2009.

[28] T. Zhong, F. N. Wong, T. D. Roberts, and P. Battle, "High performance photon-pair source based on a fiber coupled periodically poled KTiOPO$_4$ waveguide," *Opt. Express*, vol. 17, no. 14, pp. 12 019–12 030, Jul. 2009.

[29] J. Chen, A. J. Pearlman, A. Ling, J. Fan, and A. Migdall, "A versatile waveguide source of photon pairs for chip-scale quantum information processing," *Opt. Express*, vol. 17, no. 8, pp. 6727–6740, Apr. 2009.

[30] S. Tanzilli, H. De Riedmatten, W. Tittel, H. Zbinden, P. Baldi, M. De Micheli, D. B. Ostrowsky, and N. Gisin, "Highly efficient photon-pair source using periodically poled lithium niobate waveguide," *Electron. Lett.*, vol. 37, no. 1, pp. 26–28, Jan. 2001.

[31] M. C. Booth, M. Atatüre, G. Di Giuseppe, B. E. A. Saleh, A. V. Sergienko, and M. C. Teich, "Counterpropagating entangled photons from a waveguide with periodic nonlinearity," *Phys. Rev. A*, vol. 66, no. 2, p. 023815, Aug. 2002.

[32] H. Guillet de Chatellus, A. V. Sergienko, B. E. A. Saleh, M. C. Teich, and G. Di Giuseppe, "Non-collinear and non-degenerate polarization-entangled photon generation via concurrent type-I parametric downconversion in PPLN," *Opt. Express*, vol. 14, no. 21, pp. 10 060–10 072, Oct. 2006.

[33] H. Nishihara, M. Haruna, and T. Suhara, *Optical Integrated Circuits*.   New York: McGraw-Hill, 1989.

[34] B. E. A. Saleh and M. C. Teich, *Fundamentals of Photonics,* 2nd ed.   Hoboken, NJ: Wiley, 2007.

[35] A. C. Busacca, C. L. Sones, R. W. Eason, and S. Mailis, "First-order quasi-phase-matched blue light generation in surface-poled Ti:indiffused lithium niobate waveguides," *Appl. Phys. Lett.*, vol. 84, no. 22, pp. 4430–4432, May 2004.

[36] Y. L. Lee, C. Jung, Y.-C. Noh, M. Park, C. Byeon, D.-K. Ko, and J. Lee, "Channel-selective wavelength conversion and tuning in periodically poled Ti:LiNbO$_3$ waveguides," *Opt. Express*, vol. 12, no. 12, pp. 2649–2655, Jun. 2004.

[37] R. C. Alferness and R. V. Schmidt, "Tunable optical waveguide directional coupler filter," *Appl. Phys. Lett.*, vol. 33, no. 2, pp. 161–163, Jul. 1978.

[38] R. C. Alferness, "Efficient waveguide electro-optic TE $\rightleftharpoons$ TM mode converter/wavelength filter," *Appl. Phys. Lett.*, vol. 36, no. 7, pp. 513–515, Apr. 1980.

[39] J. Hukriede, D. Runde, and D. Kip, "Fabrication and application of holographic Bragg gratings in lithium niobate channel waveguides," *J. Phys. D, Appl. Phys.*, vol. 36, no. 3, pp. R1–R16, Jan. 2003.

[40] D. Runde, S. Brunken, S. Breuer, and D. Kip, "Integrated-optical add/drop multiplexer for DWDM in lithium niobate," *Appl. Phys. B: Lasers Opt.*, vol. 88, no. 1, pp. 83–88, Jun. 2007.

[41] D. Runde, S. Breuer, and D. Kip, "Mode-selective coupler for wavelength multiplexing using LiNbO$_3$:Ti optical waveguides," *Cent. Eur. J. Phys.*, vol. 6, no. 3, pp. 588–592, Sep. 2008.

[42] R. V. Schmidt and H. Kogelnik, "Electro-optically switched coupler with stepped $\Delta\beta$ reversal using Ti-diffused LiNbO$_3$ waveguides," *Appl. Phys. Lett.*, vol. 28, no. 9, pp. 503–506, May 1976.

[43] H. Kogelnik and R. V. Schmidt, "Switched directional couplers with alternating $\Delta\beta$," *IEEE J. Quantum Electron.*, vol. QE-12, no. 7, pp. 396–401, Jul. 1976.

[44] M. M. Fejer, G. A. Magel, D. H. Jundt, and R. L. Byer, "Quasi-phase-matched second harmonic generation: Tuning and tolerances," *IEEE J. Quantum Electron.*, vol. 28, no. 11, pp. 2631–2654, Nov. 1992.

[45] C. K. Hong, Z. Y. Ou, and L. Mandel, "Measurement of subpicosecond time intervals between two photons by interference," *Phys. Rev. Lett.*, vol. 59, no. 18, pp. 2044–2046, Nov. 1987.

[46] R. A. Campos, B. E. A. Saleh, and M. C. Teich, "Fourth-order interference of joint single-photon wave packets in lossless optical systems," *Phys. Rev. A*, vol. 42, no. 7, pp. 4127–4137, Oct. 1990.

[47] D. H. Jundt, "Temperature-dependent Sellmeier equation for the index of refraction, n_e, in congruent lithium niobate," *Opt. Lett.*, vol. 22, no. 20, pp. 1553–1555, Oct. 1997.

[48] K. K. Wong, Ed., *Properties of Lithium Niobate*.   Stevenage, U.K.: IEE, 2002.

[49] M. D. Feit, J. A. Fleck, Jr., and L. McCaughan, "Comparison of calculated and measured performance of diffused channel-waveguide couplers," *J. Opt. Soc. Amer.*, vol. 73, no. 10, pp. 1296–1304, Oct. 1983.

[50] S. K. Korotky and R. C. Alferness, "Ti:LiNbO$_3$ integrated optic technology," in *Integrated Optical Circuits and Components: Design and Applications*, L. D. Hutcheson, Ed.   New York: Marcel Dekker, 1987.

[51] G. B. Hocker and W. K. Burns, "Mode dispersion in diffused channel waveguides by the effective index method," *Appl. Opt.*, vol. 16, no. 1, pp. 113–118, Jan. 1977.

[52] N. Gisin, G. Ribordy, W. Tittel, and H. Zbinden, "Quantum cryptography," *Rev. Mod. Phys.*, vol. 74, no. 1, pp. 145–195, Mar. 2002.

[53] L. E. Myers, R. C. Eckardt, M. M. Fejer, R. L. Byer, W. R. Bosenberg, and J. W. Pierce, "Quasi-phase-matched optical parametric oscillators in bulk periodically poled LiNbO$_3$," *J. Opt. Soc. Amer. B*, vol. 12, no. 11, pp. 2102–2116, Nov. 1995.

[54] R. Ferriere, B.-E. Benkelfat, J. M. Dudley, and K. Ghoumid, "Bragg mirror inscription on LiNbO$_3$ waveguides by index microstructuration," *Appl. Opt.*, vol. 45, no. 15, pp. 3553–3560, May 2006.

[55] A. Norton and C. de Sterke, "Aperiodic 1-dimensional structures for quasi-phase matching," *Opt. Express*, vol. 12, no. 5, pp. 841–846, Mar. 2004.